

Rapid short-term cooling following the Chicxulub impact at the Cretaceous–Paleogene boundary

Johan Vellekoop^{a,1}, Appy Sluijs^a, Jan Smit^b, Stefan Schouten^{c,d}, Johan W. H. Weijers^{c,2}, Jaap S. Sinninghe Damsté^{c,d}, and Henk Brinkhuis^a

^aMarine Palynology, Department of Earth Sciences, Faculty of Geosciences, Laboratory of Palaeobotany and Palynology, Utrecht University, 3584 CD, Utrecht, The Netherlands; ^bEventstratigraphy, Sedimentology, Faculty of Earth- and Life Sciences, VU University Amsterdam, 1081 HV, Amsterdam, The Netherlands; ^cGeochemistry, Department of Earth Sciences, Faculty of Geosciences, Utrecht University, 3584 CD, Utrecht, The Netherlands; and ^dDepartment of Marine Organic Biogeochemistry, NIOZ Royal Netherlands Institute of Sea Research, 1790 AB, Den Burg, Texel, The Netherlands

Edited by Thure E. Cerling, University of Utah, Salt Lake City, UT, and approved April 11, 2014 (received for review October 14, 2013)

The mass extinction at the Cretaceous–Paleogene boundary, ~66 Ma, is thought to be caused by the impact of an asteroid at Chicxulub, present-day Mexico. Although the precise mechanisms that led to this mass extinction remain enigmatic, most postulated scenarios involve a short-lived global cooling, a so-called “impact winter” phase. Here we document a major decline in sea surface temperature during the first months to decades following the impact event, using TEX₈₆ paleothermometry of sediments from the Brazos River section, Texas. We interpret this cold spell to reflect, to our knowledge, the first direct evidence for the effects of the formation of dust and aerosols by the impact and their injection in the stratosphere, blocking incoming solar radiation. This impact winter was likely a major driver of mass extinction because of the resulting global decimation of marine and continental photosynthesis.

K–Pg boundary | bolide impact | Climate change | organic paleothermometry

The Cretaceous–Paleogene (K–Pg) boundary mass extinction was one of the most devastating events in the Phanerozoic history of life, both on land and in the oceans (1, 2). It is widely acknowledged to be related to the impact of an asteroid with an estimated diameter of ~10 km at Chicxulub, Yucatan Peninsula, Mexico (3–6). Impact models suggest that the first hours after the impact were characterized by earthquakes and tsunamis and the so-called “fireball stage,” including an intense heat pulse resulting from the return flux of larger ejecta, in turn resulting in global wildfires (7). Next, the dust and sulfur aerosols, originating from the anhydrite target rocks, are predicted to have partially blocked incoming solar radiation, leading to an “impact winter” (8, 9), potentially further amplified by soot derived from burning of fossil organic matter in targeted sediments, a strong absorber of short-wave radiation (10). This dark phase is proposed to have temporarily inhibited photosynthesis, causing a global collapse of terrestrial and marine food webs (5, 6).

Model simulations suggest that the amount of sunlight reaching Earth’s surface was potentially reduced to ~20% (9). This implies a ~300 W·m⁻² reduction in energy supply, which should have resulted in a severe but short-lived drop in global surface temperature (6, 11). The resulting enhanced contrast between relatively warm oceans and cold atmosphere likely fueled large storms and hurricanes (12, 13), increasing the residence time of dust in the atmosphere. In the months to decades following the impact, the atmosphere probably stabilized, and dust began to rain down and accumulate in depositional settings. This included asteroid-derived trace elements, globally recognized as a peak in platinum group element (PGE; including iridium) concentrations in complete marine and terrestrial successions (14). Crucially, fossil evidence for this impact winter scenario is still missing because this period of reduced solar radiation may only have lasted several months to decades (8, 10, 15, 16), generally too short to be captured in the ancient sedimentary record. In case of the K–Pg boundary this is even more

complicated because the traditional proxy carriers for the surface ocean conditions, calcareous microfossils, experienced major extinction (17). Furthermore, diagenetic alteration is commonly noted in postextinction biotic carbonates, inhibiting accurate temperature reconstructions (18).

Among the few sections with potentially sufficient temporal resolution across the K–Pg boundary are the exceptionally well-preserved and well-studied outcrops exposed along the Brazos River between Waco and Hearne, Texas (31° 7′53.59″N, 96°49′26.08″W; Fig. 1). In the Late Cretaceous and early Paleogene, the Brazos area was characterized by nearly continuous and predominantly siliciclastic sedimentation on the shallow shelf of the northern Gulf of Mexico, close to the entrance of the Western Interior Seaway (19, 20), at estimated depths of 75–200 m (21, 22). The sedimentary successions in this region comprise the Maastrichtian Corsicana (Kemp Clay) Formation and the Paleocene basal and upper Littig members of the Kincaid Formation.

At Brazos River, the K–Pg boundary interval has been further subdivided in a series of the lithological units (Units A to J; Fig. 2) (21, 22). The upper Maastrichtian fossiliferous shales of the Corsicana Formation (Unit A) (22, 23) are overlain by the basal part of the Paleocene Kincaid Formation, consisting of a sequence of sandstone layers yielding multiple types of clasts and shell debris (Units B, C, and D) that have been interpreted as impact-triggered tsunami deposits (21–25). The top of this sandstone complex comprises abundant burrows. The overlying complex of organic-rich silts and mudstones (Units E, F, and G)

Significance

Here, for the first time (to our knowledge), we are able to demonstrate unambiguously that the impact at the Cretaceous–Paleogene boundary (K–Pg, ~66 Mya) was followed by a so-called “impact winter.” This impact winter was the result of the injection of large amounts of dust and aerosols into the stratosphere and significantly reduced incoming solar radiation for decades. Therefore, this phase will have been a key contributory element in the extinctions of many biological clades, including the dinosaurs. The K–Pg boundary impact presents a unique event in Earth history because it caused global change at an unparalleled rate. This detailed portrayal of the environmental consequences of the K–Pg impact and aftermath aids in our understanding of truly rapid climate change.

Author contributions: J.V., J.S.S.D. and H.B. designed research; J.V., J.S., and H.B. performed research; S.S. contributed new reagents/analytic tools; J.V. and J.S. analyzed data; and J.V., A.S., J.S., S.S., J.W.H.W., J.S.S.D., and H.B. wrote the paper.

The authors declare no conflict of interest.

This article is a PNAS Direct Submission.

¹To whom correspondence should be addressed. E-mail: j.vellekoop@uu.nl.

²Present address: Royal Dutch Shell, 2288 GS, Rijswijk, The Netherlands.

This article contains supporting information online at www.pnas.org/lookup/suppl/doi:10.1073/pnas.1319253111/-DCSupplemental.

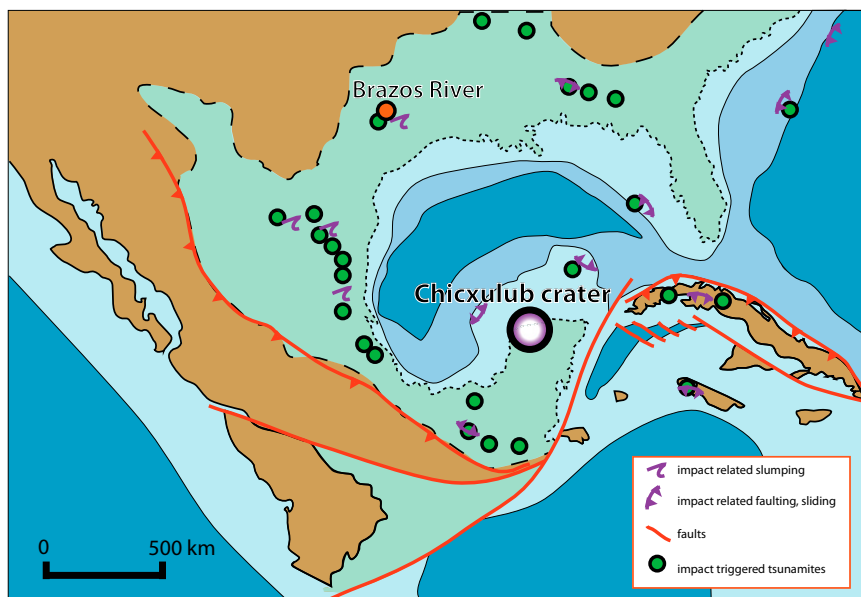


Fig. 1. A paleogeographic map of the Gulf of Mexico at the end of the Cretaceous. The Brazos-1 locality (red dot) and the Chicxulub crater are indicated, as well as other sites (green dots) with K–Pg impact-related tsunamites, slumping, faulting, and sliding compiled in ref. 22. Paleogeography based on ref. 45.

includes the Ir anomaly, consisting of scattered and smeared-out peaks of up to 2 ppb (22, 23) (*SI Age Model*).

Traditionally, the age model of the Brazos River 1 (BR1) section is based on biostratigraphy, the Ir anomaly, and the identification of impact-related tsunami beds (Fig. 3). Here we update this age model with higher-resolution planktic foraminifer and organic-walled dinoflagellate cyst (dinocyst) biostratigraphy (*SI Age Model*). We also present a grain size record to further refine the temporal sequence of events following the impact. Finally, we generated TEX_{86} paleo-sea surface temperature (SST) proxy record to assess temperature changes across the K–Pg boundary at Brazos River. The TEX_{86} paleothermometer is based on glycerol dibiphytanyl glycerol tetraether (GDGT) lipids produced by marine Thaumarchaeota (26). A full methodological description is available in *SI Materials and Methods*. Our study is the first to apply the TEX_{86} SST proxy to reconstruct very fast (decadal) changes in deep time. Critically, mesocosm and sediment trap studies have shown that in the modern ocean, the Thaumarchaeota that produce the GDGTs adjust their membrane lipids to ocean water temperatures within weeks (27, 28). Furthermore, Thaumarchaeota have been shown to be able to grow chemoautotrophically in complete darkness (27). Therefore, strong changes in SST over months to decades, as projected to have occurred during an impact winter, can be recorded using TEX_{86} .

Results and Discussion

The grain size data show that the complex of Units E, F, and G is fining upward (Fig. 2), suggesting that it was formed in a rapid depositional event (19). This material was probably initially deposited as the settling tail-end of the impact-induced tsunami/seiche (21, 22) and subsequently resuspended during postimpact storms (23, 29). Such storms might have been triggered by the enhanced contrast between warm oceans and cold atmosphere during an impact winter (13). Supporting evidence for these storms has also been found in the Geulhemmerberg section in The Netherlands, where the lowermost Danian is characterized by an alternating sequence of shell hashes and clays, interpreted to be related to episodic storm wave activity alternated with unusually low energy conditions (30). At Brazos River, the rapid deposition of the complex of Units E, F, and G would have occurred in the waning stages of such storms. Numerical model

experiments have shown that the temperature contrast causing these storms lasted for less than a century (16). Therefore, we assume that Units E, F, and G were deposited less than 100 y after the impact. The occurrence of the Ir anomaly within this complex confirms our estimation of the maximum duration of the deposition of Units E, F, and G because the settling down of PGE-bearing impact dust likely occurred on a similar timescale (31). Modern-day examples of dust input by volcanic eruptions, burning oil wells, and nuclear bomb testing resulted in settling times of months to years (32–35). Various studies have indicated that with high-energy events such as nuclear explosions and asteroid impacts, black carbon particles and aerosols are knocked into the upper stratosphere, where they quickly spread globally and produce a long-lasting climate forcing (35). With these kinds of events, particles and aerosols end up much higher than, for example, volcanic aerosols, which typically end up just above the tropopause (32). As a result, aerosols produced by large impacts will have a residence time that is considerably longer than those produced by, for example, volcanos and burning oil wells.

Some of these estimates do not include the time it takes for particles to sink from the sea surface to the seafloor, which significantly prolongs the settling time for the very fine fraction to which the impact-derived PGEs are believed to be associated (14, 31). Moreover, the proposed extraordinary large storms during the initial impact winter phase might have temporarily resuspended material, both in the atmosphere and in the ocean, further delaying the deposition of PGE-bearing impact dust. As a result, previous studies have resulted in a wide range of different estimated settling times, ranging from <10 y up to >10 kyr, although these latter values seem improbable because mechanisms to keep particles suspended for such prolonged periods of time appear lacking (31). With estimated water depths of 75–200 m (21, 22), settling time of PGE-bearing impact dust will have been in the order of 1–100 y at the Brazos River site. The scattered nature of the Ir record, combined with the dinocyst assemblages, implies that the complex of Units E, F, and G reflects a mixture of earliest Paleocene and reworked uppermost Maastrichtian materials. Given the time required to deposit the iridium on the sea floor and given the presence of burrows in the top of the underlying tsunami deposited sandstone Unit D, the rapid deposition of this mixture eventually took place years to decades after the impact. Therefore, although mixed,

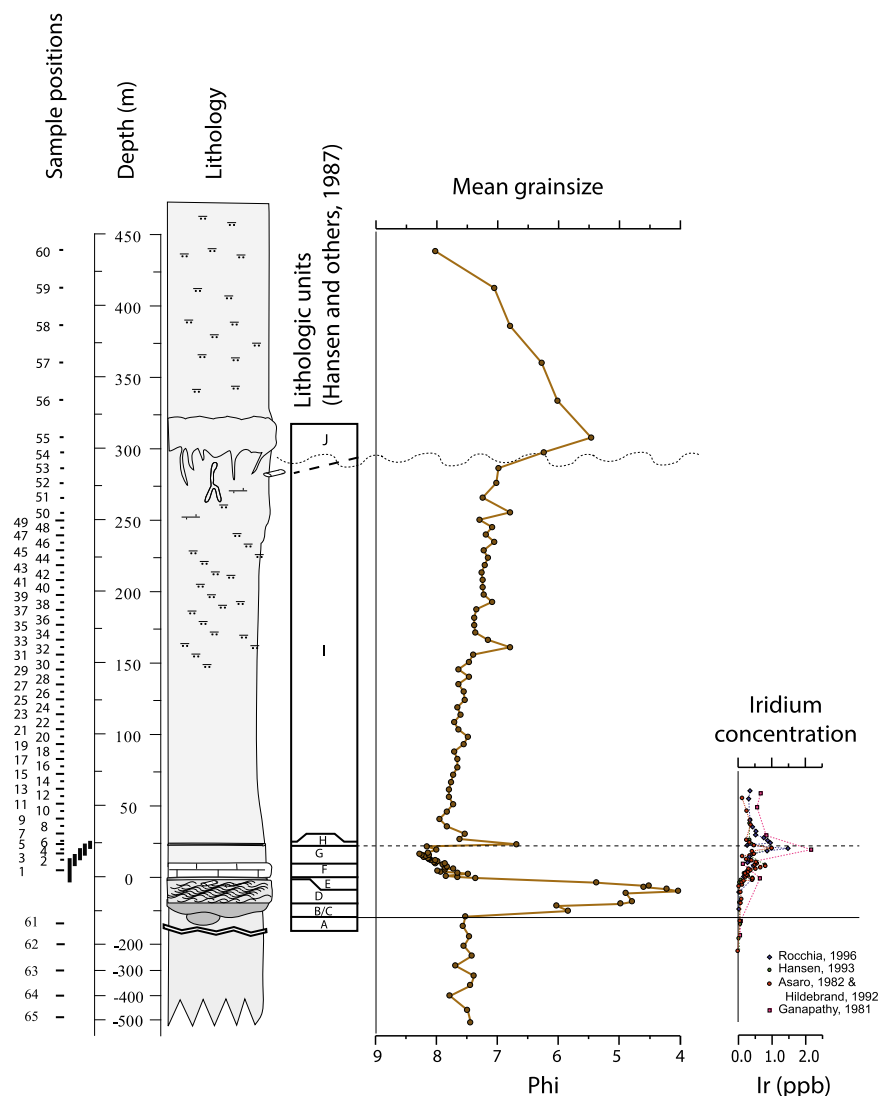


Fig. 2. Sample positions of the 1995 sample set, plotted with lithological units, mean grain size on the Krumbein phi (ϕ) scale, and four different Iridium profiles, from refs. 46–49. A closely spaced sample set was obtained to acquire a high temporal resolution.

the complex of Units E, F, and G provides a unique insight in the environmental conditions in the first decades following the K–Pg boundary impact.

Our TEX_{86} proxy record can be subdivided in three phases/intervals (I–III; Fig. 3). Interval I shows that Uppermost Cretaceous SSTs were stable and high, with values of ~ 30 – 31 °C using the $\text{TEX}_{86}^{\text{H}}$ calibration (36), in agreement with published proxy records and climate model simulations for the Upper Cretaceous (37, 38). Within the tsunami deposits, TEX_{86} values cannot be used to reconstruct SST because of high concentrations of terrestrially derived GDGTs (39) (*SI Application of TEX_{86}*). However, in the section directly above the main tsunami deposits (Units E, F, and G; interval II) a distinct cooling phase is recorded, with average SSTs up to 2 °C lower than preimpact values and two significant drops of up to 7 °C below preimpact values. In the subsequent Interval III, SSTs are generally 1–2 °C higher than those for the preimpact deposits.

The most remarkable features in our data are the two prominent drops in SST in the postimpact, mixed tsunami–storm deposits. As indicated above, this interval, and likely also the GDGTs, represents a mixture of redeposited uppermost Maastrichtian and immediate postimpact materials that was eventually deposited within the settling tail of tsunami activity and in the

waning stage of the postimpact storms. Variable amount of mixing of reworked uppermost Maastrichtian GDGTs with basal Paleocene postimpact GDGTs might explain the multiple peaks of both our TEX_{86} record and the Ir profiles. The chaotic nature of the basal Paleocene TEX_{86} record contrasts with relatively stable and warm uppermost Maastrichtian SSTs. Hence, the samples that yield the lowest SSTs probably represent a mixture of uppermost Maastrichtian and direct postimpact GDGTs with a relatively high abundance of postimpact materials, causing substantially lower TEX_{86} values. Considering the stable and warm uppermost Maastrichtian, the immediate postimpact SSTs must have been substantially lower. Because rapid deposition of the complex of Units E, F, and G occurred within 100 y after the impact, the cooling recorded in these units likely happened in the first months to decades following the K–Pg impact. Our SST record thus provides, to our knowledge, the first evidence for a transient, global impact winter after the K–Pg boundary impact. The duration of this cold spell is in agreement with coupled ocean–atmosphere model results, suggesting that impact-induced dust and aerosol loading will result in lower SSTs for several decades, even after most of the dust has been removed from the atmosphere (40). Our results of short-term cooling following the

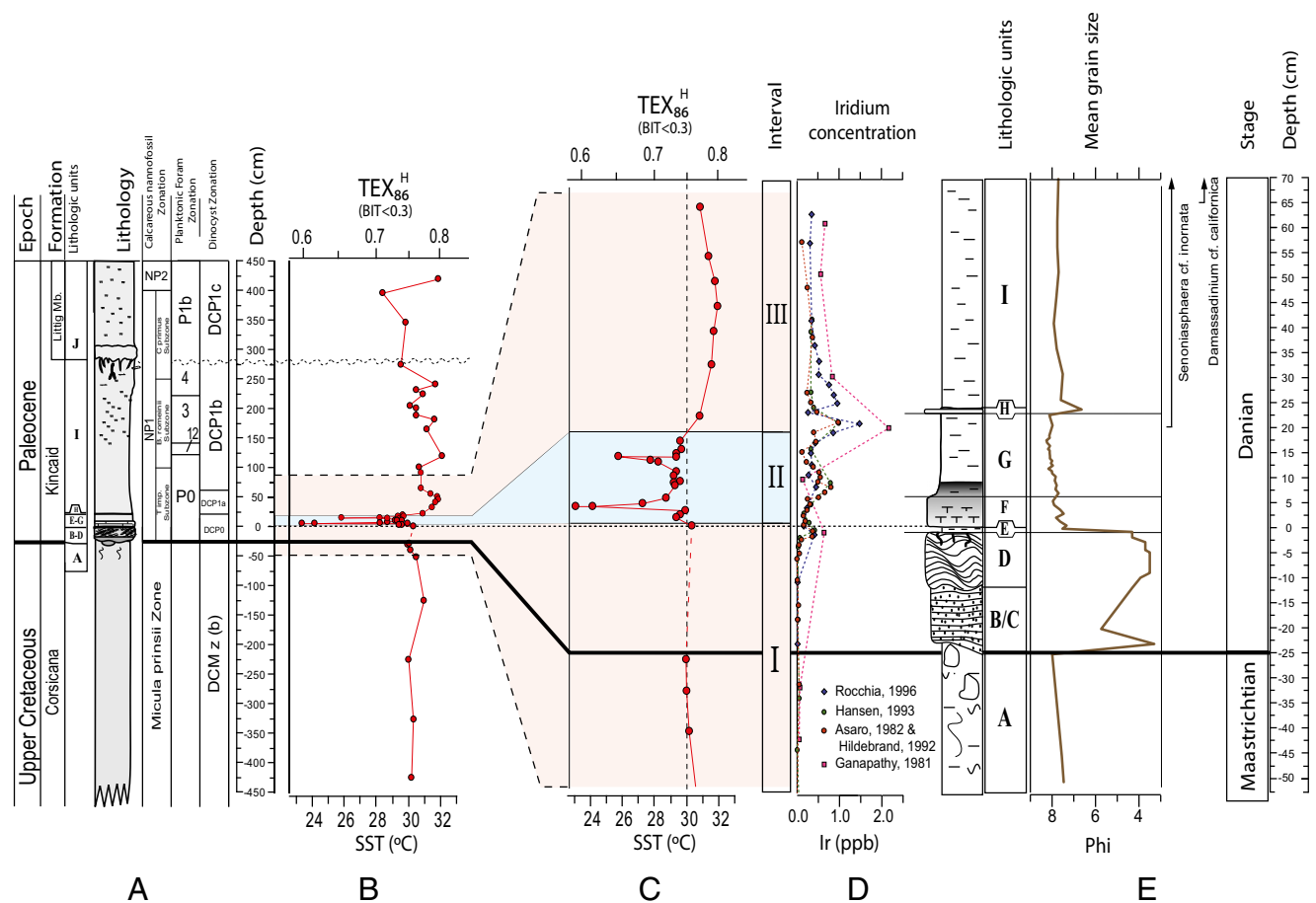


Fig. 3. Age model, TEX_{86}^H , and grain size results at the Brazos-1 section. (A) Lithostratigraphy and biostratigraphy, including calcareous nannofossil, planktic foraminifera, and dinocyst biostratigraphy, at Brazos-1. (B) TEX_{86}^H -based paleo-SST reconstruction. (C) Zoom of the TEX_{86}^H record across the K–Pg boundary interval. (D) Four different Ir records across the K–Pg boundary interval at Brazos-1, from refs. 46–49 (*SI Age Model*). (E) Lithology and grain size distribution on the Krumbein phi (ϕ) scale across the K–Pg boundary interval and first appearance datums of the first Danian dinocyst marker species.

K–Pg asteroid impact are supported by a migration of cool, boreal dinoflagellate species into the subtropic Tethyan realm directly across the K–Pg boundary interval (16, 41) and the ingress of boreal benthic foraminifera into the deeper parts of the Tethys Ocean, interpreted to reflect millennial timescale changes in ocean circulation following the impact, attributed to a hypothesized short-term cooling of 1–10 y (16).

The global impact winter, characterized by darkness and a dramatic cooling of ocean surface waters, perturbed a relatively stable, warm, latest Cretaceous climate (37) and likely represented a major stress factor for life on Earth. Therefore, it is expected to have been a key contributory element in the mass extinction at the K–Pg boundary. Additionally, when the large amount of aerosols injected into the atmosphere rained out, they might have resulted in acidification of the surface oceans (42), a further stressor for surface-dwelling organisms. The initial cooling was followed by a long-term warming trend (41), also observed in our TEX_{86} record (Fig. 2) and in previously reported stable isotope analyses (43), that most likely is associated with greenhouse gases released into the atmosphere from the vaporization of carbonate target rock, the mass mortality, and forest fires (6, 8, 10, 41). Our study reveals a combination of environmental and climatological events that is compatible with the pattern of extinction of many biological clades, including most species of planktic foraminifera and many coccolithophorids but also larger marine taxa like ammonites and marine reptiles, in addition to the dinosaurs and flying reptiles (1, 2, 16).

Materials and Methods

For TEX_{86} analyses, freeze-dried, powdered samples (~10 g dry mass) were extracted with an accelerated solvent extractor using a 9:1 (vol/vol) dichloromethane (DCM):methanol solvent mixture. The obtained extracts were separated over an activated Al_2O_3 column, using 9:1 (vol/vol) hexane:DCM, ethyl acetate (100%), 95:5 (vol/vol) DCM:MeOH, and 1:1 (vol/vol) DCM:methanol, into apolar, ethylacetate, and tetraether and polar fractions, respectively. The tetraether fractions were analyzed by HPLC/APCI-MS (HPLC/atmospheric pressure positive ion chemical ionization mass spectrometry) using an Agilent 1100 series Liquid Chromatography/Mass Spectrometric Detector type SL. TEX_{86} indices were calculated and converted into temperature estimates as described in *SI Materials and Methods*.

For palynological analyses, oven-dried samples (~10–15 g dry mass) were spiked with Lycopodium spores to facilitate the calculation of absolute palynomorph abundances. Chemical processing comprised treatment with 10% HCl and 40% HF for carbonate and silica removal, respectively. Ultrasonication was used to disintegrate palynodebris. Residues were sieved over a 15- μ m mesh and mounted on microscope slides, which were analyzed at 200 \times and 1,000 \times magnification to a minimum of 200 dinocysts. A detailed, step-by-step processing protocol is given in *SI Materials and Methods*. Taxonomy used follows that cited in the Lentin and Williams Index of Fossil Dinoflagellates, 2004 (44), unless stated otherwise. See *SI Taxonomic Notes on Organic-Walled Dinoflagellate Cysts* for taxonomical notes. All slides are stored in the collection of the Laboratory of Paleobotany and Palynology, Utrecht University.

For analyses of planktic foraminifera, standard micropaleontological techniques were applied (*SI Materials and Methods*).

The grain size distribution was determined on a Fritsch A-22 laser particle sizer (*SI Materials and Methods*).

ACKNOWLEDGMENTS. E. Hopmans and J. Ossebaer (NIOZ Royal Netherlands Institute of Sea Research) are thanked for analytical assistance with TEX86 analyses. Funding for this research was provided by Utrecht University and

the Netherlands Organization for Scientific Research Open Competition Grant ALW/PJ09047 (to H.B. and J.S.S.D.). A.S. acknowledges the European Research Council for Starting Grant 259627.

- Bambach RK (2006) Phanerozoic biodiversity mass extinctions. *Annu Rev Earth Planet Sci* 34:127–155.
- Alroy J (2008) Colloquium paper: Dynamics of origination and extinction in the marine fossil record. *Proc Natl Acad Sci USA* 105(Suppl 1):11536–11542.
- Alvarez LW, Alvarez W, Asaro F, Michel HV (1980) Extraterrestrial cause for the Cretaceous-Tertiary extinction. *Science* 208(4448):1095–1108.
- Smit J, Hertogen J (1980) An extraterrestrial event at the Cretaceous-Tertiary boundary. *Nature* 285(5753):198–200.
- Schulte P, et al. (2010) The Chicxulub asteroid impact and mass extinction at the Cretaceous-Paleogene boundary. *Science* 327(5970):1214–1218.
- Kring DA (2007) The Chicxulub impact event and its environmental consequences at the Cretaceous-Tertiary boundary. *Palaeogeogr Palaeoclimatol Palaeoecol* 255(1-2): 4–21.
- Robertson DS, McKenna MC, Toon OB, Hope S, Lillegraven JA (2004) Survival in the first hours of the Cenozoic. *Geol Soc Am Bull* 116(5-6):760–768.
- Pierazzo E, Kring DA, Melosh HJ (1998) Hydrocode simulation of the Chicxulub impact event and the production of climatically active gases. *J Geophys Res* 103(E12): 28607–28625.
- Pope KO, Baines KH, Ocampo AC, Ivanov BA (1997) Energy, volatile production, and climatic effects of the Chicxulub Cretaceous/Tertiary impact. *J Geophys Res* 102(E9): 21645–21664.
- Harvey MC, Brassell SC, Belcher CM, Montanari A (2008) Combustion of fossil organic matter at the Cretaceous-Paleogene (K-P) boundary. *Geology* 36(5):355–358.
- Pierazzo E, Hahmann AN, Sloan LC (2003) Chicxulub and climate: Radiative perturbations of impact-produced S-bearing gases. *Astrobiology* 3(1):99–118.
- Emanuel KA, Speer K, Rotunno R, Srivastava R, Molina M (1995) Hypercanes: A possible link in global extinction scenarios. *J Geophys Res* 100(D7):13755–13765.
- Covey C, Thompson SL, Weissman PR, MacCracken MC (1994) Global climatic effects of atmospheric dust from an asteroid or comet impact on Earth. *Global Planet Change* 9(3-4):263–273.
- Claeys P, Kiessling W, Alvarez W (2002) Distribution of Chicxulub ejecta at the Cretaceous-Tertiary Boundary. *Spec Pap Geol Soc Am* 356:55–69.
- Pope KO, Baines KH, Ocampo AC, Ivanov BA (1994) Impact winter and the Cretaceous/Tertiary extinctions: Results of a Chicxulub asteroid impact model. *Earth Planet Sci Lett* 128(3-4):719–725.
- Galeotti S, Brinkhuis H, Huber M (2004) Records of post-Cretaceous-Tertiary boundary millennial-scale cooling from the western Tethys: A smoking gun for the impact-winter hypothesis? *Geology* 32(6):529–532.
- Hull PM, Norris RD, Bralower TJ, Schueth JD (2011) A role for chance in marine recovery from the end-Cretaceous extinction. *Nat Geosci* 4(12):856–860.
- Magaritz M, Benjamini C, Keller G, Moshkovitz S (1992) Early diagenetic isotopic signal at the Cretaceous Tertiary boundary, Israel. *Palaeogeogr Palaeoclimatol Palaeoecol* 91(3-4):291–304.
- Davidoff AJ, Yancey TE (1993) Eustatic cyclicity in the Paleocene and Eocene: Data from the Brazos River valley, Texas. *Tectonophysics* 222(3-4):371–395.
- Kennedy WJ, Landman NH, Christensen WK, Cobban WA, Hancock JM (1998) Marine connections in North America during the late Maastrichtian: Paleogeographic significance of *Jeletzkytes nebrascensis* Zone cephalopod fauna from the Elk Butte Member of the Pierre Shale, SE Dakota and NE Nebraska. *Cretac Res* 19(6):745–775.
- Bourgeois J, Hansen TA, Wiberg PL, Kauffman EG (1988) A tsunami deposit at the Cretaceous-Tertiary boundary in Texas. *Science* 241(4865):567–570.
- Smit J, et al. (1996) Coarse-grained, clastic sandstone complex at the K/T boundary around the Gulf of Mexico: Deposition by tsunami waves induced by the Chicxulub impact? *Geol Soc Am Spec Pap* 307:151–182.
- Hansen TA, Farrand RB, Montgomery HA, Billman HG, Blechschmidt GL (1987) Sedimentology and extinction patterns across the Cretaceous-Tertiary boundary interval in East Texas. *Cretac Res* 8(3):229–252.
- Schulte P, Speijer R, Mai H, Kontny A (2006) The Cretaceous-Paleogene (K-P) boundary at Brazos, Texas: Sequence stratigraphy, depositional events and the Chicxulub impact. *Sediment Geol* 184(1-2):77–109.
- Smit J, Romein AJT (1985) A sequence of events across the Cretaceous-Tertiary boundary. *Earth Planet Sci Lett* 74(2-3):155–170.
- Schouten S, Hopmans EC, Schefuss E, Sinninghe Damsté JS (2002) Distributional variations in marine crenarchaeotal membrane lipids: A new organic proxy for reconstructing ancient sea water temperatures? *Earth Planet Sci Lett* 204(1):265–274.
- Wuchter C, Schouten S, Coolen MJL, Sinninghe Damsté JS (2004) Temperature-dependent variation in the distribution of tetraether membrane lipids of marine Crenarchaeota: Implications for TEX86 paleothermometry. *Paleoceanography* 19(4):PA4208.
- Wuchter C, Schouten S, Wakeham SG, Sinninghe Damsté JS (2006) Archeal tetraether membrane lipid fluxes in the northeastern Pacific and the Arabian Sea: Implications for TEX₈₆ paleothermometry. *Paleoceanography* 21(4):PA4208.
- Hart MB, et al. (2012) The Cretaceous-Paleogene boundary on the Brazos River, Texas: New stratigraphic sections and revised interpretations. *GCAGS J* 1:69–80.
- Smit J, Brinkhuis H (1996) The Geulhemmerberg Cretaceous/Tertiary boundary section (Maastrichtian type area, SE Netherlands); summary of results and a scenario of events. *Geol Mijnb* 75(2-3):283–293.
- Kring DA, Durda DD (2002) Trajectories and distribution of material ejected from the Chicxulub impact crater: Implications for postimpact wildfires. *J Geophys Res* 107(E8): 5062.
- Oman L, et al. (2006) Modeling the distribution of the volcanic aerosol cloud from the 1783–1784 Laki eruption. *J Geophys Res* 111(D12):D12209.
- Mackinnon IDR, Gooding JL, McKay DS, Clanton US (1984) The E1 Chichón stratospheric cloud: Solid particulates and settling rates. *J Volcanol Geotherm Res* 23(1-2): 125–146.
- Hobbs PV, Radke LF (1992) Airborne studies of the smoke from the Kuwait oil fires. *Science* 256(5059):987–991.
- Robock A, Oman L, Stenchikov GL (2007) Nuclear winter revisited with a modern climate model and current nuclear arsenals: Still catastrophic consequences. *J Geophys Res* 112(D13):D13107.
- Kim JH, et al. (2010) New indices and calibrations derived from the distribution of crenarchaeal isoprenoid tetraether lipids: Implications for past sea surface temperature reconstructions. *Geochim Cosmochim Acta* 74(16):4639–4654.
- Pearson PN, et al. (2001) Warm tropical sea surface temperatures in the Late Cretaceous and Eocene epochs. *Nature* 413(6855):481–487.
- Donnadieu Y, Pierrehumbert R, Jacob R, Fluteau F (2006) Modelling the primary control of paleogeography on Cretaceous climate. *Earth Planet Sci Lett* 248(1-2): 426–437.
- Weijers JWH, Schouten S, Spaargaren OC, Sinninghe-Damsté JS (2006) Occurrence and distribution of tetraether membrane lipids in soils: Implications for the use of the TEX86 proxy and the BIT index. *Org Geochem* 37(12):1680–1693.
- Luder T, Benz W, Stocker TF (2002) Modeling long-term climatic effects of impacts: First results. *Geol Soc Am Spec Pap* 356:717–729.
- Brinkhuis H, Bujak JP, Smit J, Versteegh GJM, Visscher H (1998) Dinoflagellate-based sea surface temperature reconstructions across the Cretaceous-Tertiary boundary. *Palaeogeogr Palaeoclimatol Palaeoecol* 141(1-2):67–83.
- D'hondt S, Pilson MEQ, Sigurdsson H, Hanson AK, Carey S (1994) Surface-water acidification and extinction at the Cretaceous-Tertiary boundary. *Geology* 22(11):983–986.
- Romein AJT, Smit J (1981) The Cretaceous-Tertiary boundary: Calcareous nannofossils and stable isotopes. *Proc K Ned Akad Wet* 84:295–314.
- Fensome RA, Williams GL (2004) *The Lentin and Williams Index of Fossil Dinoflagellates 2004 Edition*. American Association of Stratigraphic Palynologists Contributions Series 42.
- Stéphan JF, et al. (1990) Paleogeodynamic maps of the Caribbean: 14 steps from Lias to Present. *Bull Soc Geol Fr* 8(6):915–919.
- Ganapathy R, Gartner S, Jiang M-J (1981) Iridium anomaly at the Cretaceous-Tertiary boundary in Texas. *Earth Planet Sci Lett* 54(3):393–396.
- Hansen TA, Upshaw B III, Kauffman EG, Gose W (1993) Patterns of molluscan extinction and recovery across the Cretaceous-Tertiary boundary in east Texas: Report on new outcrops. *Cretac Res* 14(6):685–706.
- Asaro F, Michel HV, Alvarez W, Alvarez LW, Maddocks RF, Bunch T (1982) Iridium and other geochemical profiles near the Cretaceous-Tertiary boundary in a Brazos river section in Texas. *Texas ostracoda, International Symposium on Ostracoda, 8th, Guidebook of Excursion and Related Papers*, ed Maddocks RF (Univ of Houston, Houston), pp 238–241.
- Rocchia R, Robin E, Froget L, Gayraud J (1996) Stratigraphic distribution of extraterrestrial markers at the Cretaceous-Tertiary boundary in the Gulf of Mexico area: Implications for the temporal complexity of the event. *Spec Pap Geol Soc Am* 307: 279–286.